Article

Cite This: Biomacromolecules 2019, 20, 769−777

pubs.acs.org/Biomac

Binding Forces of Cellulose Binding Modules on Cellulosic Nanomaterials

Alessandra Griffo,[†] Bart J. M. Rooijakkers,[†] Hendrik Hähl,[‡] Karin Jacobs,[‡] Markus B. Linder,[†] and Päivi Laaksonen*[,†]

[†]Department of Bioproducts and Biosystems, Aalto University, Espoo, FI-00076 Aalto, Finland

[‡]Department of Experimental Physics, Saarland University, Saarbrücken 66123, Germany

Supporting Information

ABSTRACT: In this study, the interaction forces between different cellulosic nanomaterials and a protein domain belonging to cellulose binding modules family 1 (CBM1) were investigated at the molecular scale. Cellulose binding modules are protein domains found in carbohydrate active enzymes having an affinity toward cellulosic materials. Here, the binding force of a fusion protein containing a cellulose binding module (CBM1) produced recombinantly in *E. coli* was quantified on different cellulose nanocrystals immobilized on surfaces. Adhesion of the CBM on cellulose with different degrees of crystallinity as well as on chitin nanocrystals was examined. This study was carried out by single molecule force spectroscopy using an atomic force microscope, which enables the detection of binding force of individual molecules. The study contains a preliminary quantification of the interactions at the molecular level that sheds light on the development of new nanocellulose-based nanocomposites with improved strength and elasticity.

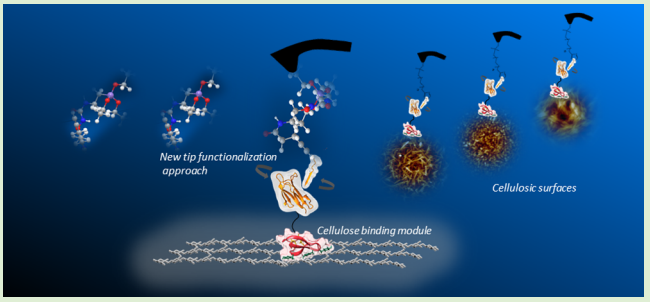

1. INTRODUCTION

Cellulose is the most abundant biopolymer in Nature and plays an important role in the structures of many plants. Certain organisms, such as fungi, bacteria, and algae, have developed special enzymes that selectively degrade cellulose and turn it into sugars that the organism itself can readily consume as nutrition.[1] These enzymes, namely cellulases, contain cellulose binding modules (CBMs) that are able to selectively anchor the actual enzyme to cellulose.[2] The majority of these domains have carbohydrate-binding activity; they are classified to different families according to the amino acid sequence similarity. Family I CBMs are small (typically 36 amino acids), protein modules with two highly conserved disulfide bridges and asymmetric shape with one side serving as the binding surface. What is less commonly acknowledged, but has a major importance, is that binding modules much like the cellulose binding modules also exist at the interfaces of biological composite structures such as nacre[3] and squid beak.[4] These interfacial components play a very important role in promoting adhesion between the components of these hybrid materials. They can be particularly interesting for the design of high performance materials as composites of high mechanical resilience and as a tool in bioengineering.[5,6] Previous studies showed how coupling engineered proteins containing CBMs as interlinking architectures with stiffer materials can tune the mechanical properties of the designed architecture.[6,7]

The carbohydrate-binding activity of CBMs on cellulose fibers from different origins has been widely studied in recent years[8−10] with a focus on understanding the enzymatic hydrolysis of the renewable lignocellulosic biomass[11] and for the development of hydrolase kinetic models.[12] Degradation of cellulose by microbial enzymes has also been considered an important biological and industrial process to produce environmentally friendly biofuels.[8] There are also studies employing CBM-terminated proteins as binding modules between cellulosic nanomaterials.[7,13]The strategy mimics interfacial design of biological nanocomposites, where bonding through biomolecular interactions is able to sacrifice individual bonds in order to prevent damage on a larger scale. An example of such is found in the human body, where the collagen filaments located between the bones absorb impacts, "sacrificing" their own intramolecular bonds, in the same way that the CBMs are supposed to work as building blocks that dissipate the energy caused by stress between nanocellulose surfaces.[14]

Among the CBMs, the Cel7A-CBM1 is an attractive choice as an anchoring unit for functional surfaces due to its high binding affinity on cellulose.[10] The three aromatic residues of the down face of Cel7A-CBM1 represent the driving interaction for binding to cellulose (Figure 1). The interaction between CBM1 and cellulose is a combination of stacking of aromatic residues due to π-electron interactions and hydrogen

Received: September 7, 2018
Revised: January 9, 2019
Published: January 18, 2019

DOI: 10.1021/acs.biomac.8b01346
Biomacromolecules 2019, 20, 769−777

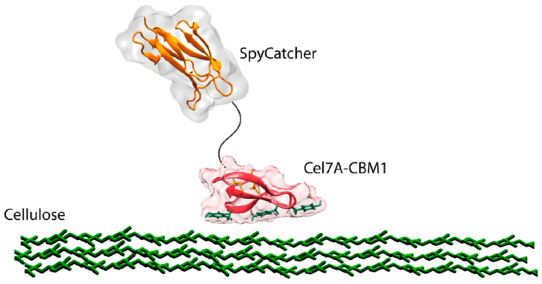

Figure 1. Side view of the fusion protein SpyCatcher-Cel7A-CBM1 interacting with a cellulosic surface. SpyCatcher domain (orange) is linked to the CBM1 (red) via a linker (black).

bonding, which together cause specificity between the CBM and a cellulosic crystal.[15] Figure 1 presents a side view of the binding of a single Cel7A-CBM1 domain accompanied by the fusion partner SpyCatcher on top of the cellulose surface. In order to obtain surfaces with biomolecular function having a molecular level precision in orientation, fusion proteins produced using recombinant DNA techniques, together with selective chemical conjugation, can be employed.

The binding strength of CBM1 from the *Trichoderma reesei* cellulase Cel7A[20,21] was quantified by measuring the strength of adhesion between the CBM and cellulosic surfaces having different chemical composition and crystallinity at nanoscale resolution by single molecule force spectroscopy.[22] Due to their topicality and current interest as a building block for nanocomposites, we have chosen to focus on nanocellulosic materials and the differences between them. AFM images of cellulosic surface functionalized with these proteins are reported in Figure SI 1.

The force spectroscopy experiments were carried out by connecting a fusion protein of SpyCatcher and Cel7A-CBM1 to the tip of an atomic force microscope (AFM) covalently through a polymeric linker. The fusion protein was produced as a recombinant fusion protein (SpyCatcher-Cel7A-CBM1) that was attached to the AFM tip functionalized with a peptide dubbed SpyTag (Figure 2). SpyCatcher is a protein fragment derived from the splitting of immunoglobulin-like collagen adhesion domain (CnaB2) in two components (SpyCatcher and SpyTag) that are able to link together via spontaneous formation of an amide bond between SpyCatcher *Lys* and SpyTag *Asp* side chains.[16] Click chemistry reactions, which are high yielding and quickly form new strong covalent bonds, have been widely used to functionalize AFM tips[17−19] whereas the usage of the SpyTag-SpyCatcher bond for this purpose is quite novel.

2. MATERIALS AND METHODS

2.1. Protein Expression and Purification. The Smt3-SpyCatcher-SAlinker-Cel7A-His6 plasmid was cotransformed into chemically competent BL21(DE3) *E. coli* cells with CyDisCo plasmid pMJS205[23] (which was employed to ensure the formation of disulfide bridges in the CBM1 domain). One colony was picked and used to grow a preculture in LB medium supplemented with kanamycin (50 mg L^{-1}) and chloramphenicol (35 mg L^{-1}), overnight at 37 °C with shaking. 500 mL of MagicMedia expression medium (ThermoFischer) were supplemented with kanamycin (50 mg L^{-1}) and chloramphenicol (35 mg L^{-1}), inoculated with 1:10 of the preculture, and grown for 24 h at 30 °C, 230 rpm.

The cells were then harvested by centrifugation (24 471*g* (rotor radius 15.2 cm), 4 °C, 10 min), removal of the media and resuspended in lysis buffer (20 mM NaH_2PO_4, 20 mM imidazole, 500 mM NaCl, 100 μg mL^{-1} fresh lysozyme, 20 μg mL^{-1} DNase I, 20 μg mL^{-1} $MgCl_2$, protease inhibitor cocktail (Sigma-Aldrich) at 4 °C. After 30 min shaking at 4 °C, the cell suspension was further lysed by running it 2 times through an EmulsiFlex-C3 homogenizer (Avestin, Inc.), after which the cell debris was removed by centrifugation (24 471*g*, rotor radius 15.2 cm, 4 °C, 25 min).

The resulting lysate was incubated with the protease Ulp1 for 1 h at room temperature to cleave off the Smt3 domain. The proteins were subsequently purified using a GE healthcare ÄKTA Pure LC system with HisTrap IMAC columns.

SpyCatcher-His6 ("plain" SpyCatcher protein) was produced using the same method, only omitting the CyDisCo plasmid and the cleaving with Ulp1 (no Smt3). The pure proteins were verified by SDS-PAGE analysis with Coomassie Blue staining and MALDI-TOF mass spectrometry (Bruker). Protein concentrations were determined

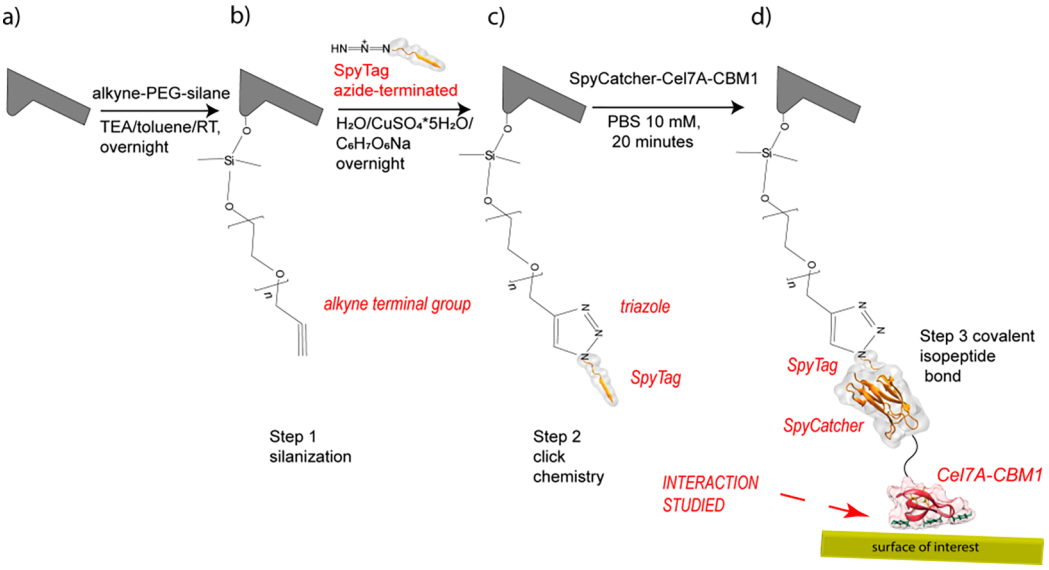

Figure 2. Schematic of the tip functionalization process, in which three steps of reaction are required: the bare tip is first functionalized by (a) silanization and then (b) a SpyTag azide terminated peptide reacts with the alkyne group of the alkyne-PEG-silane (c) and eventually the SpyTag peptide reacts with the SpyCatcher terminated fusion protein forming a strong covalent isopeptide bond (d).

DOI: 10.1021/acs.biomac.8b01346
Biomacromolecules 2019, 20, 769−777

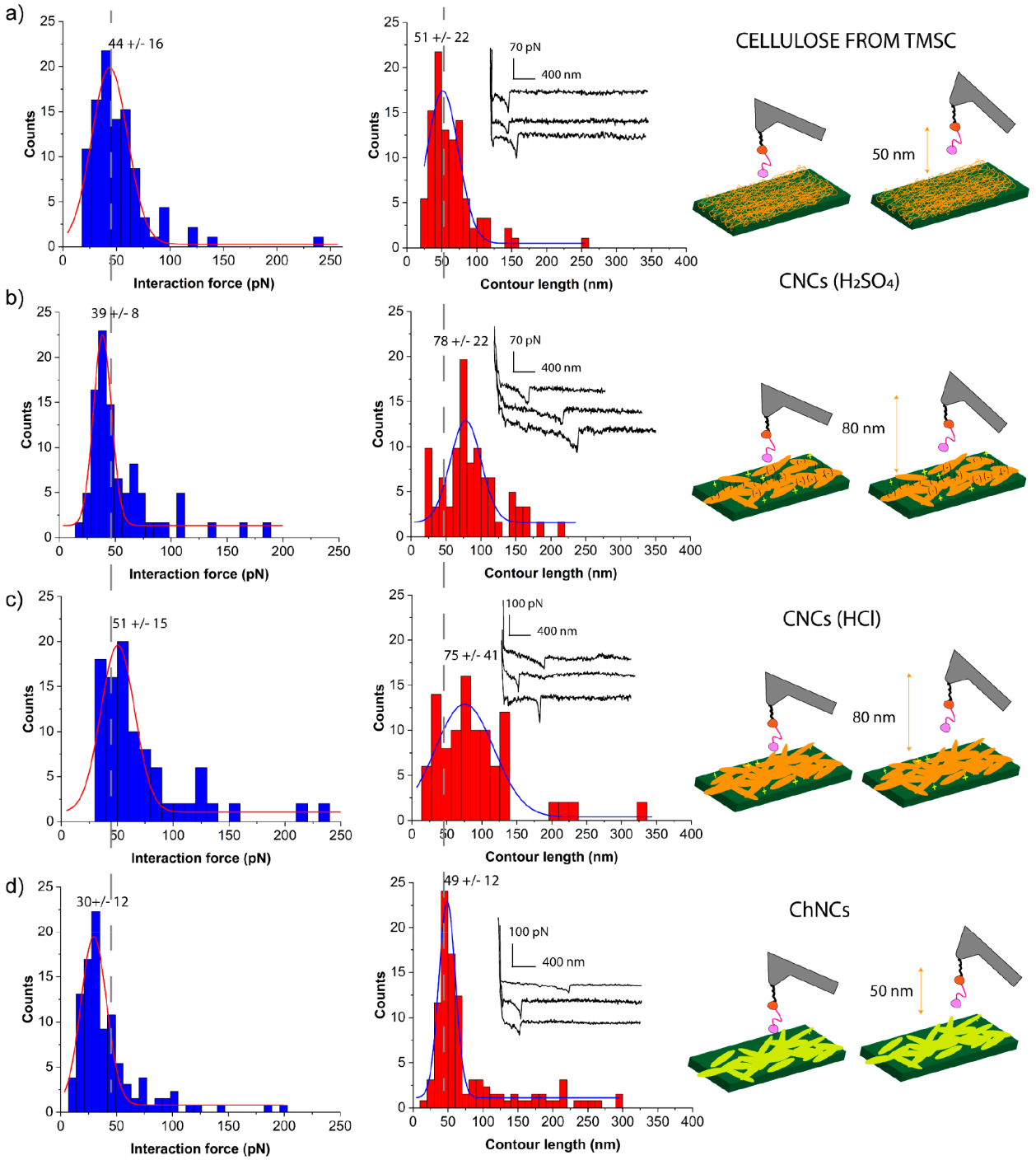

Figure 3. Histograms representing the binding interaction force (blue bars) and the contour length (red bars) respectively for cellulose from TMSC (n = 96) (a), cellulose nanocrystals (CNCs) from sulfuric acid hydrolysis (n= 64) (b), cellulose nanocrystals (CNCs) from hydrochloric acid hydrolysis (n=57) (c), Chitin nanocrystals (ChNCs) (n=129) (d). Additional FD curves on CNC showing multiple rupture events in which not a single molecule but more detachment events happen, are excluded from the analysis as well as the ones in which the fit was not perfectly applicable. Histograms summing such curves to the one here presented are reported in Figure SI 4. Dotted grey lines are used as a guide to the eye for pointing out the differences between the obtained values in respect to the TMSC sample. On the right: Schematic representation of the SMFS experiment for each system studied.

by measuring the absorption at 280 nm using a Varian Cary 50 UV−vis spectrophotometer, corrected for background and calculated using the extinction coefficient, predicted based on a protein sequence by ProtParam.[24] More information about the plasmid design and preparation are reported in the Supporting Information (Figure SI 2).

2.2. Tip Functionalization. The SpyCatcher-Cel7A-CBM1 was covalently bound to an AFM tip through a multistep functionalization process (Figure 2) consisting of a silanization reaction (step 1), a click chemistry reaction (step 2), and the SpyTag-Spycatcher isopeptide bond formation[16] (step 3). Steps 1 and 2 are adapted by the procedure described elsewere.[25]

Before functionalization, the Si_2N_3 tips (MLCT-D, 0.03 N m^{-1} spring constant, Bruker) were treated with a UV-ozonator to make them hydrophilic, then immersed in a solution of toluene containing 0.1 mM alkyne-PEG-silane solution (3.4 kDa, NANOCS) in the presence of trimethylamine 0.5 mM (TEA) (99%, Sigma-Aldrich) as

DOI: 10.1021/acs.biomac.8b01346
Biomacromolecules 2019, 20, 769−777

catalyst, and left overnight. Afterward, the tips were gently rinsed with toluene and immersed in an aqueous solution containing a 10 μM azide labeled SpyTag peptide (<40%, Biomatik), sodium ascorbate (≥99%, Sigma-Aldrich), and copper sulfate pentahydrate (≥98%, Sigma-Aldrich) respectively in a ratio of 4:2:1. After 24 h, the tips were gently rinsed with Milli-Q water. Then 50 μL of 1 μM protein solution were cast on it for 15 min and rinsed with phosphate-buffered saline 10 mM (PBS) (NaCl, BioXtra, ≥99.5%; NaH_2PO_4 BioXtra, ≥99.0% ; KH_2PO_4, ≥99.0% (Sigma); KCl, BioXtra, ≥99.0% (Sigma-Aldrich)). PBS has been described as one of the best solvents to quickly activate the SpyTag-SpyCatcher reaction.[17] The protein casting was performed 30 min before each AFM experiment, whereas the silanized and SpyTag-functionalized tips could be prepared within a week before the experiment.

2.3. Preparation of the Surfaces. *2.3.1. Cellulosic and Chitin Surfaces.* Regenerated cellulose, chitin, and cellulose nanocrystals thin films were all prepared by spin coating (Laurell WS 650SX-6NPP/LITE).

In detail, the regenerated cellulose was prepared as described elsewhere.[26] Briefly, a trimethylsilyl cellulose (TMSC, purity >98%, kindly donated by Prof. Dr. Thomas Heinze, Friedrich Schiller University Jena) solution in toluene was spin coated on a cleaned SiO_2 substrate (sonication in ethanol, acetone, and water followed by UV-ozonator treatment for 5 min) at the speed 4400 rpm and acceleration 2200 rms^{-1} for 45 s and then converted to cellulose by exposure to hydrochloric acid (HCl) 12 M (Sigma-Aldrich) vapor for 3 min.

Chitin nanocrystals (ChNCs) were prepared from purified chitin flakes from shrimp shells (Sigma-Aldrich) by a 90 min hydrolysis with 3 M HCl at 90 °C. Subsequently, the acid residue was washed out and the ChNCs were further purified by dialysis for 2 days, after which the pH of the suspension was adjusted to pH 4 with 1 M HCl. The degree of acetylation of the ChNCs was calculated from ^{13}C NMR spectra to be 99.6%. The resulting ChNCs dispersion with a solid content of 5 mg mL^{-1} was first sonicated with a tip sonicator (power 20%, time 20 min pulse on/off, Bransor Digital Sonifier, tapered microtip) and then spin coated (100 μL at 4400 rpm, 2200 rms^{-1} for 45 s) on a SiO_2 surface that has been cleaned with plasma.

Cellulose nanocrystals (CNCs) from sulfuric acid H_2SO_4 hydrolysis, prepared as described elsewhere,[27] at a concentration of 6 mg mL^{-1} were spin coated (4400 rpm and 2200 rms^{-1} for 45 s) on a 0.5 mg mL^{-1} PEI coated SiO_2, previously left to adsorb for 15 min and rinsed with Milli-Q water[28,29]

Eventually, cellulose nanocrystals (CNCs) from HCl hydrolysis (kindly donated by Prof. Eero Kontturi, Aalto University) were prepared as described elsewhere.[30] In detail, first 0.5 mg mL^{-1} polyethylenimine (PEI) was spin coated (100 μL, 3000 rpm, 1260 rms^{-1}, 40 s) on SiO_2 and rinsed with Milli-Q water three times by spin coating at the same spinning conditions.[31] Afterward, CNCs (HCl) were spin coated at a concentration of 10 mg mL^{-1} at the same spinning conditions.

2.4. Single Molecule Force Spectroscopy Measurements. The experiments were carried out with a Bruker Multimode 8 instrument, sample immersed in 10 mM PBS buffer, using MLCT-D cantilevers (0.03 N m^{-1} spring constant). For each experiment at least 500−600 single force/distance curves were recorded and then analyzed. Only the specific single adhesion curves were chosen for the fitting and the analysis. The force measurements were carried out using a ramp size of 500 nm, a scan rate of 0.5 Hz, a forward and reverse velocity of 500 nm s^{-1} (loading rate 15 × 10^3 pN), and a relative force trigger of 108 pN. The data were processed using homemade MATLAB scripts for baseline and contact point correction and extraction of the rupture force of the first adhesion signal. Moreover, to the first peak in a force vs surface separation data representation of the data the wormlike chain model (eq 1)[32] was fitted which describes the chain as a semiflexible polymer chain with the free parameters persistence length, l_P, and contour length of the chain, l_C.

$$F(z) = \frac{k_B T}{l_P}\left(\frac{z}{l_C} + \frac{1}{4(1 - {}^{z}/_{l_C})^2} - \frac{1}{4}\right) \quad (1)$$

2.5. AFM Imaging. Topographical images were recorded by AFM (Bruker multimode 8) in tapping mode in air. The images were scanned using silicon cantilevers (HQ:NSC, tip radius 8 nm, MikroMasch) with a resonance frequency of 325 kHz and a force constant of 40 N m^{-1}. The scanned image sizes were (2 μm)^2.

2.6. Fourier Transform Infrared Spectroscopy with Attenuated Total Reflectance. Fourier transform infrared spectroscopy measurements based on attenuated total reflectance (ATR-FT-IR) (Nicolet iS50 FT-IR, ThermoScientific) were recorded in a dry environment under total attenuated reflectance conditions by pressing the samples against the Germanium crystal plate. The acquisition spectra range was 600−4000 cm^{-1}, 64 scans, ATR correction. Three measurements for each sample were performed. Background correction is applied to all the spectra with the ThermoScientific Omnic sofware.

2.7. Water Contact Angle Measurements. The water contact angle (WCA) was measured using the sessile drop method (KSV, Biolin Scientific), with 5 μL water droplets.

3. RESULTS

3.1. Single Molecule Force Spectroscopy Experiments. The single molecule force spectroscopy (SMFS) experiments were carried out by approaching the surface of interest with the SpyCatcher-Cel7A-CBM1 coated tip, and hundreds of approaching and retracting cycles were repeated. On average around 4−20% of the recorded curves showed specific adhesion, 50−80% showed no adhesion, and 20−50% showed nonspecific adhesion. The percentages for the experiments carried out on the different surfaces and examples of the F_d curves corresponding to each case are reported in Table S1 and Figure SI 3. All the retraction curves, denoted as F_d, showing a specific binding peak, have been analyzed with the wormlike chain model, and the data are shown as histograms in Figure 3a−d, representing the interaction force and the contour length.

Once the tip functionalization was verified (see the sections below), SpyCatcher-Cel7A-CBM1 binding with cellulose was investigated by measuring the force−distance responses by AFM. The Cel7A-CBM1 exhibited binding forces in the range 30−60 pN on the different cellulosic surfaces (see Figure 3). However, small variations were observed; the binding forces of Cel7A-CBM1 to the $CNC_{(H_2SO_4)}$, $CNC_{(HCl)}$, and TMSC-derived cellulose were 39 ± 8 pN, 51 ± 15 pN, and 44 ± 16 pN, respectively. The largest difference was between the two types of CNCs. The Gaussian distribution of $CNC_{(HCl)}$ and TMSC-cellulose fell instead in the similar range 44−51 pN. Differences were also noted in the contour lengths corresponding to the detachment of the SpyCatcher-Cel7A-CBM1 that were extracted from the F_d curves. While the 75 ± 41 nm and 78 ± 22 nm contour lengths were measured on the CNC surface from both origins, the regenerated cellulose reached its most frequent value at 51 ± 22 nm. From calculation based on the number of amino acids of the whole polymer chain length, *including Alkyne-PEG-silane, SpyTag, and SpyCatcher fusion protein* (Table SI 2), the theoretical length estimated for the protein chain was 40−50 nm, being close to the observed one for the interaction with regenerated cellulose. However, there was some variation in the length of the PEG linker, due to its polydispersity.[33]

For observing the binding to a substrate with high similarity to cellulose, a surface coated with chitin nanocrystals was

DOI: 10.1021/acs.biomac.8b01346
Biomacromolecules 2019, 20, 769−777

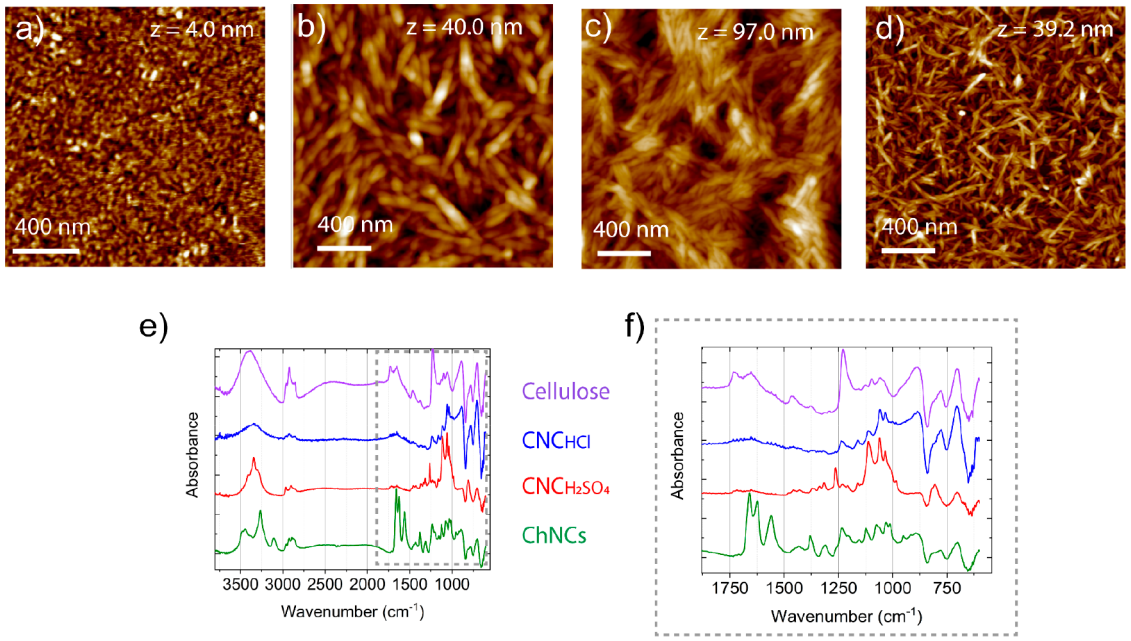

Figure 4. AFM images of (a) cellulose from TMSC, (b) ChNCs, (c) $CNC_{(HCl)}$, and (d) $CNC_{(H2SO4)}$. (e) FT-IR spectra of the samples. (f) Zoomed region highlighted by the dashed gray rectangle in (e). The SiO_2 background was subtracted in all the spectra.

studied. The recorded force curves fell in a range similar to the single molecule binding on cellulose with a slightly smaller rupture force (30 ± 12 pN) and matching contour length (49 nm ±12) (Figure 3d).

Getting only one protein attachment on the AFM tip required using a low protein concentration. For the cellulosic surfaces, a 1 μM protein concentration was used. An example of an experiment using a 10 μM protein concentration is shown in the Supporting Information (Figure SI 5), and the retraction curves consist of multiple detachment peaks attributed to a larger number of interacting molecules. On the other hand, a protein concentration of 10 μM was suitable for obtaining single detachment peaks on the chitin surfaces (Figure SI 5).

3.2. Morphology and Chemical Analysis of the Model Surfaces. All the studied surfaces were characterized in terms of morphology, roughness, and chemical composition. First, AFM pictures were recorded (Figure 4a–d). Cellulose from hydrolyzed TMSC showed a network-like structure of low roughness (R_q = 0.56). The cellulose nanocrystals from HCl and H_2SO_4 hydrolysis as well as the chitin nanocrystals showed instead a higher roughness (respectively R_q = 13.9, R_q = 5.9, and R_q = 6.19) due to the random assembly of the crystals deposited on the surface. The CNCs resulting from HCl hydrolysis were clearly bundled, whereas the sulfonated CNCs were dispersed as single crystals. Different CNCs deposition methods were performed in order to obtain uniform coverage and reduce the roughness (Figure SI 6). The best arrangement was achieved by using the cationic polyelectrolyte polyethylenimine (PEI) as a fixing layer below the CNCs.

The samples were also characterized by ATR-FT IR (Figure 4e and f). CNCs showed the characteristic peaks of cellulose: the broad band at 3400–3300 cm^{-1} due to the OH stretching, the peaks at 2907 cm^{-1} due to the aliphatic saturated CH-stretching in the glucose units, and 1164 cm^{-1} corresponding to the asymmetrical bridge C–O–C stretching.[34,35] The area between 1200 and 850 cm^{-1} is attributed to the glucopyranose ring,[36] but we observed in the spectra of Figure 4e a slight shift around 850–1250 cm^{-1}. For the sulfonated CNCs, the symmetric stretching of the sulfate ester linkages (S–O–C) was displayed at 811 cm^{-1} (peak highlighted by the dashed brown circle). ChNCs instead showed the characteristic peaks due to the amide bands (1654, 1621, 1554 cm^{-1}), OH stretching vibrations (3444 cm^{-1}), N–H (3103 cm^{-1}), and CH2 and CH3 (2885 cm^{-1}) stretching.[37] The observed peaks are listed in Table 1.

Table 1. Estimated Values of TCI for the Surfaces Studied

Surface	TCI ($I_{1375\ cm^{-1}}/I_{2900\ cm^{-1}}$)
Cellulose	0.1
CNC(HCl)	0.5
CNC(H_2SO_4)	0.7
ChNCs	–

FT-IR spectra have been also used in order to deduct the crystallinity of the mentioned surfaces. In fact, according to a theory developed in 1962[38,39] it is possible to estimate the total crystallinity index (TCI) by the ratio of the intensity of the peaks recorded at 1372 and 2900 cm^{-1} (1375/2900 cm^{-1}). The assumption for which of those peaks were chosen is that the region between 1200 and 1400 cm^{-1} contains several bands affected by the amorphous content of the sample rather than by the lattice type, whereas the band at 2900 cm^{-1} is supposed to be unaffected by changes in crystallinity. Furthermore, the band at 898 cm^{-1} is assigned to the amorphous region in cellulose,[40] and is most prominent in cellulose. The band at around 1420–1430 cm^{-1} is indeed associated with the amount of the crystalline structure of the cellulose, but the signal is weak in all the spectra so we could not calculate the lateral order index (LOI) based on the intensity ratio (1420/1893 cm^{-1}). The estimated TCIs are reported in Table 1.

3.3. Force Distance Curves of Functionalized Tip and Control Experiments. Control experiments were performed

DOI: 10.1021/acs.biomac.8b01346
Biomacromolecules 2019, 20, 769–777

to guarantee the success of the tip functionalization in the force spectroscopy measurements. In addition to the interaction between cellulose and SpyCatcher-Cel7A-CBM1 fusion protein (Figure 5a), also the force between cellulose and the AFM tip functionalized with plain SpyCatcher without Cel7A-CBM1 was studied (Figure 5b).

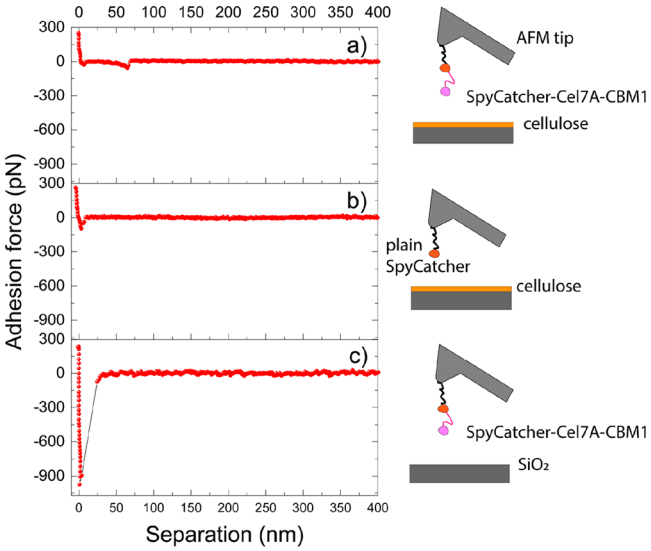

Figure 5. F_d curves with the related schematic representing the interaction between SpyCatcher-Cel7A-CBM1 and cellulose (a), plain SpyCatcher and cellulose (b), and SpyCatcher- Cel7A-CBM1 and SiO_2 (c).

A second control experiment was to measure the nonspecific interaction between the Cel7A-CBM1-functionalized tip and SiO_2 surface (Figure 5c). The peaks recorded for the CBM could be identified as single molecule adhesion peaks due to their magnitude (tens of pN) and the contour length matching the molecules dimensions. The SpyCatcher instead did not show any specific adhesion on cellulose, and the nonspecific adhesion peak located around 0 nm differed only in terms of the absolute force value from the one of SpyCatcher-Cel7A-CBM1 on cellulose. In fact, the interaction force of the plain SpyCather was around 100 pN and that of SpyCatcher-Cel7A-CBM1 on SiO_2 was typically more than 400 pN (ca. 1 nN in Figure 5c).

The stepwise functionalization of the AFM tip and the related force responses on the contact with cellulose surface are presented in Figure SI 7. The F_d curves measured between the bare tip and a cellulose sample (Figure SI 7a) showed only the nonspecific adhesion peak located at 0 nm of separation indicating that no specific binding or stretching between the tip and surface happened. Subsequently, the same experiment on the cellulose surface was repeated with the alkyne functionalized tip (Figure SI 7b) and the SpyTag functionalized tip (Figure SI 7c). This time molecular rupture peaks were observed for both, distinguishable in interaction force (52 pN for the SpyTag and 184 pN for the alkyne) and contour length (27 nm for the SpyTag and 64 nm for the alkyne). The SiO_2 surfaces were also studied by contact angle measurements and FT-IR to further ensure the success of steps 1 and 2 (Figure SI 8).

4. DISCUSSION

4.1. Binding of SpyCatcher-Cel7A-CBM1 on Cellulosic and Chitin Surfaces. The SpyCatcher-Cel7A-CBM1 adheres to cellulose through the three π-electron rich tyrosine groups that are exposed to the binding face of the protein. Structural studies indicate that the spacing of the three aromatic residues coincides with the spacing of every second glucose ring on a cellulose chain[41,42] meaning that the binding occurs between the aromatic rings and the pyranose rings exposed on the (110) crystalline face of cellulose.[43−45] This sets a limitation for the ability to bind to cellulose with chemical substitution. Our nanocrystals present a sulfur content of 278 mmol·kg^{-1} or 0.33%S (determined by conductometric titration;[27,46] see Figure SI 9), slightly lower than the typical sulfur contents reported for the sulfuric acid hydrolyzed CNCs near 0.6%,[27,47] meaning that about 6−7% of the hydroxyls groups of the cellulose surface are substituted by sulfate groups. The sulfate groups may cause steric and electrostatic repulsion to a CBM, which would optimally bind to a nonderivatizes cellulose surface where there are no functional groups other than the hydroxlys, and thus lead to a weaker binding.

Indeed, binding to the nonderivatized CNC(HCl) was tens of pNs stronger than on the sulfate-derivatized cellulose nanocrystals CNC(H2SO4). Moreover, comparison of the approaching curves for both types of CNCs (Figure SI 10) reveals that there is more repulsion extending to near 30 nm in the case of the sulfate-derivatized CNCs.

In addition to short-range forces, also the hydration forces, described as a general repulsive mechanism associated with ordering of water at an interface,[48] may contribute. The negatively charged CNCs tend to bind more water molecules (by charge−dipole and dipole−dipole interactions) than the neutral polysaccharide (by dipole−dipole interactions) highlighting that there may be a difference in the hydration repulsion between the two types of CNCs. However, since the hydration interactions occur within a very short distance, we cannot observe them with the accuracy of the method and it is not possible to distinguish that from the electrostatics, since all the repulsion interactions add up in the force−distance curves.

The nonderivatized cellulosic surfaces had very similar interaction force values, which indicates that neither the surface morphology nor the crystallinity played a significant role in the binding force. The similarity of the chemical composition of the cellulose model surface and $CNC_{(HCl)}$ was high (Figure 4e−f), but the regenerated cellulose is highly amorphous,[49] whereas the CNCs are very crystalline (see Table 1). Finding that the crystallinity did not affect the binding force was surprising, and it encourages the use of different types of celluloses for building materials employing the CBM as an adhesive molecule.

The contour length measured at the different cellulose surfaces, however, showed some differences between the samples. For the surfaces of nanocrystals, the contour lengths had typically larger values and a wider distribution with a less regular shape. There were four possible sources for the unusually high rupture distances that apparently exceeded the length of the molecule, two of them related to the cellulose surfaces and two with the tip functionalization. (1) The roughness of the CNC surfaces was high, also confirmed by the AFM scans (Figure 4). This caused variation on the surface level, and consequently the height where the AFM tip contacted the surface was less well-defined compared to the

DOI: 10.1021/acs.biomac.8b01346
Biomacromolecules 2019, 20, 769−777

smooth cellulose film. Therefore, also the detachment of the tip-bound proteins may have occurred at slightly different height levels, resulting in larger rupture distances and a wider distribution of the contour lengths (see also Figure SI4). (2) Second, the CNCs were not chemically fixed to the surface, but only held together by the van der Waals forces and hydrogen bonds between the CNC surfaces. The random orientation of the CNCs did not guarantee a high contact area between individual crystals and in some experiments, especially with $CNC_{(HCl)}$ and ChNC, the crystals may have been lifted by the AFM probe while retracting, resulting in contour lengths exceeding 200 nm (Figure 2c and d). (3) The tip functionalization through silanization includes a possibility of uncontrolled attachment of the PEG on the tip surface. The silane may have formed a thin layer of gel, which caused variation in the linker length. (4) The PEG-linker polydispersity[33] may have also caused variation in tens of nm during the stretching. Since the focus of the study is not on the extension behavior of the protein chain, but more on the interaction forces, we accepted the presence of these uncertainties in the comparison of the force data.

For binding to chitin, one narrow rupture force distribution at 30 ± 12 pN was observed (Figure 2d). The rupture force was expectedly weaker compared to any cellulosic surfaces. When compared to an earlier observed binding between the chitin binding domain and chitin surfaces (60−90 pN),[50] the binding force of SpyCatcher-Cel7A-CBM1 on chitin was substantially weaker, but still significant. This highlights the delicate molecular design of the carbohydrate binding domains and their specificity toward certain substrates.

There are previous studies describing the use of engineered cellulose binding proteins in composites of cellulosic nanomaterials.[6,51,52] For instance, the binding affinity of single and double Cel7A-CBM1 on cellulose nanofibers (CNF) and bacterial cellulose has been measured by isotherm binding tests that revealed differences between the two different cellulosic surfaces showing a higher affinity to CNF.[15] In many cases, the affinity of the CBMs on certain cellulosic substrates have been quantified, but considered only without the contribution of the binding forces in the mechanical and rheological properties of the systems. The binding strength of the CBM on cellulose or chitin surfaces appeared to qualitatively follow the substrate specificity of the SpyCatcher-Cel7A-CBM1, since cellulose is the primary substrate.

4.2. Binding of the SpyTag and Alkyne-PEG-Silane. The rupture forces obtained for the AFM tip functionalized with the alkyne-terminated PEG linker (Step 1 in Figure 2) on the cellulose surface were high (Figure SI 7) and may be explained by the multiple hydrogen bonds forming between the PEG linker and the cellulose surface. The PEG linker contained approximately 49 units, enabling formation of hydrogen bonds with the hydroxyl groups of the cellulose when in contact. These interactions were effectively shielded in the functionalization steps 2 and 3 (Figure SI 7). The high contour lengths of the alkyne-PEG-silane, observed in some unbinding events, may be due to the stretching of the PEG units that happens for forces up to 100 pN.[33,53]

The force curves of the tip after the functionalization step 2, where the SpyTag was exposed, appeared as single-molecule rupture curves. The specific binding of the SpyTag on cellulose may be due to the presence of tyrosine, which could bind to cellulose through π-stacking, and to hydrogen bonds or electrostatic interactions due to the two lysines. SpyTag is a small peptide (the theoretically estimated length is 5.4 nm); hence, no steric hindrance may hide such residues exposed to the interface. The contour length determined for the SpyTag experiments was near 27 nm, which was significantly lower than that for the CBM experiments. It is also interesting to note that once the SpyTag was attached on the tip, the percentage of the large force peaks attributed to the PEG linker decreased dramatically.

5. CONCLUSIONS

This study quantified the interaction forces between cellulose binding proteins and nanocelluloses. We demonstrated a new strategy for carrying out single molecule force spectroscopy experiments employing a combination of click-chemistry and protein engineering. A fusion protein consisting of the cellulose binding module of Cel7A enzyme coupled with a SpyCatcher protein was attached to an AFM tip via covalent bond and its specific binding to both amorphous cellulose, two types of cellulose nanocrystals as well as chitin nanocrystals were investigated. The attachment of the target molecule was accomplished via silanization, which appeared not to be an optimal method; thus, the obtained results are preliminary in nature. SpyCatcher-Cel7A-CBM1 had a similar interaction force (44−51 pN) on the surfaces of unmodified cellulose, although they varied by the degree of crystallinity and morphology. The binding force on the sulfate-functionalized cellulose nanocrystals was slightly lower (39 pN) than on the nonmodified surfaces (44−51 pN). Eventually, the substrate specificity of the Cel7A-CBM1 was tested by measuring the binding forces on chitin nanocrystals. The weakest interaction of 30 pN has been observed for the binding with chitin nanocrystals.

■ ASSOCIATED CONTENT

Supporting Information

The Supporting Information is available free of charge on the ACS Publications website at DOI: 10.1021/acs.biomac.8b01346.

AFM height and phase images of the fusion protein studied, sketch of the designed construct, additional F_d curves for CBM1(Cel7A)−cellulose interaction, table reporting the n experiments with the related concentrations and percentages, F_d curves for the CBM1(Cel7A)−cellulose and chitin interaction at higher concentration, AFM phase images of cellulose nanocrystals CNC prepared at different contidions, F_d curves and histograms for the stepwise tip functionalization process, AFM images and FT-IR spectra for the stepwise surface functionalization process, table reporting the theoretically estimated length of the peptides and proteins studied (PDF)

■ AUTHOR INFORMATION

Corresponding Author

*Current e-mail: paivi.laaksonen@hamk.fi.

ORCID

Markus B. Linder: 0000-0002-7271-6441

Päivi Laaksonen: 0000-0003-2029-5275

Author Contributions

The manuscript is written through contributions of all authors. A.G.: experiment design, sample preparation, measurements,

DOI: 10.1021/acs.biomac.8b01346
Biomacromolecules 2019, 20, 769−777

data analysis, writing of manuscript. B.R.: preparation and expression of the fusion proteins. M.L.: experiment design, writing of manuscript. H.H.: matlab code elaboration, help in data analysis. K.J.: writing of manuscript. P.L.: experiment design, writing of manuscript, project supervision. All authors have given approval to the final version of the manuscript.

Notes

The authors declare no competing financial interest.

■ ACKNOWLEDGMENTS

The authors would like to sincerely acknowledge financial support from the Aalto University CHEM Graduate School Programme, Academy of Finland and Center of Excellence in Molecular Engineering of Biosynthetic Hybrid Materials (HYBER), as well as Dr. Roberto Milani and VTT Technical Research Centre of Finland for the FT-IR instrument use. H.H. and K.J. acknowledge support from the German Research Foundation (DFG) in the framework of the Collaborative Research Center SFB 1027. Cellulose nanocrystals were a kind gift from Prof. Eero Kontturi. We also thank Dr. Juán Valle Delgado for the fruitful scientific discussions about the force measurements and Dr. Claudia Pigliacelli for the help in taking SEM images.

■ ABBREVIATIONS

CBMs, cellulose binding modules; CNCs, cellulose nanocrystals; FT-ATR, Fourier Transform Attenuated Total Reflectance; TMSC, trimethylsilylcellulose; PEI, polyethylenimine; PBS, phosphate buffer saline

■ REFERENCES

(1) Lynd, L. R.; Weimer, P. J.; van Zyl, W. H.; Pretorius, I. S. Microbial Cellulose Utilization: Fundamentals and Biotechnology. *Microbiol. Mol. Biol. Rev.* **2002**, *66* (3), 506−577.

(2) Linder, M.; Teeri, T. T. The Cellulose-Binding Domain of the Major Cellobiohydrolase of Trichoderma Reesei Exhibits True Reversibility and a High Exchange Rate on Crystalline Cellulose. *Proc. Natl. Acad. Sci. U. S. A.* **1996**, *93* (22), 12251−12255.

(3) Suzuki, M.; Saruwatari, K.; Kogure, T.; Yamamoto, Y.; Nishimura, T.; Kato, T.; Nagasawa, H. An Acidic Matrix Protein, Pif, Is a Key Macromolecule for Nacre Formation. *Science* **2009**, *325*, 1388−1390.

(4) Tan, Y.; Hoon, S.; Guerette, P. A.; Wei, W.; Ghadban, A.; Hao, C.; Miserez, A.; Waite, J. H. Infiltration of Chitin by Protein Coacervates Defines the Squid Beak Mechanical Gradient. *Nat. Chem. Biol.* **2015**, *11* (7), 488−495.

(5) Rosa, A. M. M.; Louro, A. F.; Martins, S. A. M.; Inácio, J.; Azevedo, A. M.; Prazeres, D. M. F. Capture and Detection of DNA Hybrids on Paper via the Anchoring of Antibodies with Fusions of Carbohydrate Binding Modules and ZZ-Domains. *Anal. Chem.* **2014**, *86* (9), 4340−4347.

(6) Laaksonen, P.; Walther, A.; Malho, J.-M.; Kainlauri, M.; Ikkala, O.; Linder, M. B. Genetic Engineering of Biomimetic Nanocomposites: Diblock Proteins, Graphene, and Nanofibrillated Cellulose. *Angew. Chem., Int. Ed.* **2011**, *50* (37), 8688−8691.

(7) Malho, J.-M.; Arola, S.; Laaksonen, P.; Szilvay, G. R.; Ikkala, O.; Linder, M. B. Modular Architecture of Protein Binding Units for Designing Properties of Cellulose Nanomaterials. *Angew. Chem., Int. Ed.* **2015**, *54* (41), 12025−12028.

(8) Zhang, M.; Wang, B.; Xu, B. Measurements of Single Molecular Affinity Interactions between Carbohydrate -Binding Modules and Crystalline Cellulose Fibrils. *Phys. Chem. Chem. Phys.* **2013**, *15* (17), 6508−6515.

(9) Qin, C.; Clarke, K.; Li, K. Interactive Forces between Lignin and Cellulase as Determined by Atomic Force Microscopy. *Biotechnol. Biofuels* **2014**, *7*, 65.

(10) Rooijakkers, B. J. M.; Ikonen, M. S.; Linder, M. B. Fungal-Type Carbohydrate Binding Modules from the Coccolithophore Emiliania Huxleyi Show Binding Affinity to Cellulose and Chitin. *PLoS One* **2018**, *13*, e0197875.

(11) Zhang, M.; Wu, S.-C.; Zhou, W.; Xu, B. Imaging and Measuring Single-Molecule Interaction between a Carbohydrate-Binding Module and Natural Plant Cell Wall Cellulose. *J. Phys. Chem. B* **2012**, *116* (33), 9949−9956.

(12) King, J. R.; Bowers, C. M.; Toone, E. J. Specific Binding at the Cellulose Binding Module−Cellulose Interface Observed by Force Spectroscopy. *Langmuir* **2015**, *31* (11), 3431−3440.

(13) Malho, J.-M.; Ouellet-Plamondon, C.; Rüggeberg, M.; Laaksonen, P.; Ikkala, O.; Burgert, I.; Linder, M. B. Enhanced Plastic Deformations of Nanofibrillated Cellulose Film by Adsorbed Moisture and Protein-Mediated Interactions. *Biomacromolecules* **2015**, *16* (1), 311.

(14) Fantner, G. E.; Hassenkam, T.; Kindt, J. H.; Weaver, J. C.; Birkedal, H.; Pechenik, L.; Cutroni, J. A.; Cidade, G. A. G.; Stucky, G. D.; Morse, D. E.; Hansma, P. K. Sacrificial Bonds and Hidden Length Dissipate Energy as Mineralized Fibrils Separate during Bone Fracture. *Nat. Mater.* **2005**, *4* (8), 612−616.

(15) Arola, S.; Linder, M. B. Binding of Cellulose Binding Modules Reveal Differences between Cellulose Substrates. *Sci. Rep.* **2016**, *6*, 35358.

(16) Zakeri, B.; Fierer, J. O.; Celik, E.; Chittock, E. C.; Schwarz-Linek, U.; Moy, V. T.; Howarth, M. Peptide Tag Forming a Rapid Covalent Bond to a Protein, through Engineering a Bacterial Adhesin. *Proc. Natl. Acad. Sci. U. S. A.* **2012**, *109* (12), E690−E697.

(17) Senapati, S.; Manna, S.; Lindsay, S.; Zhang, P. Application of Catalyst-Free Click Reactions in Attaching Affinity Molecules to Tips of Atomic Force Microscopy for Detection of Protein Biomarkers. *Langmuir* **2013**, *29* (47), 14622−14630.

(18) Chen, G.; Ning, X.; Park, B.; Boons, G.-J.; Xu, B. Simple, Clickable Protocol for Atomic Force Microscopy Tip Modification and Its Application for Trace Ricin Detection by Recognition Imaging. *Langmuir* **2009**, *25* (5), 2860−2864.

(19) Escorihuela, J.; Marcelis, A. T. M.; Zuilhof, H. Click Chemistry: Metal-Free Click Chemistry Reactions on Surfaces (Adv. Mater. Interfaces 13/2015). *Adv. Mater. Interfaces* **2015**, *2* (13), DOI: 10.1002/admi.201570063.

(20) Linder, M.; Mattinen, M.-L.; Kontteli, M.; Lindeberg, G.; Ståhlberg, J.; Drakenberg, T.; Reinikainen, T.; Pettersson, Gör.; Annila, A. Identification of Functionally Important Amino Acids in the Cellulose-Binding Domain of Trichoderma Reesei Cellobiohydrolase I. *Protein Sci.* **1995**, *4* (6), 1056−1064.

(21) Guo, J.; Catchmark, J. M. Binding Specificity and Thermodynamics of Cellulose-Binding Modules from Trichoderma Reesei Cel7A and Cel6A. *Biomacromolecules* **2013**, *14* (5), 1268−1277.

(22) Janshoff, A.; Neitzert, M.; Oberdörfer, Y.; Fuchs, H. Force Spectroscopy of Molecular Systems—Single Molecule Spectroscopy of Polymers and Biomolecules. *Angew. Chem., Int. Ed.* **2000**, *39* (18), 3212−3237.

(23) Gaciarz, A.; Veijola, J.; Uchida, Y.; Saaranen, M. J.; Wang, C.; Hörkkö, S.; Ruddock, L. W. Systematic Screening of Soluble Expression of Antibody Fragments in the Cytoplasm of E. Coli. *Microb. Cell Fact.* **2016**, *15* (1), 22.

(24) Gasteiger, E.; Hoogland, C.; Gattiker, A.; Duvaud, S.; Wilkins, M. R.; Appel, R. D.; Bairoch, A. Protein Identification and Analysis Tools on the ExPASy Server. In *The Proteomics Protocols Handbook*; Humana Press: 2005; pp 571−607.

(25) Yameen, B.; Ali, M.; Álvarez, M.; Neumann, R.; Ensinger, W.; Knoll, W.; Azzaroni, O. A Facile Route for the Preparation of Azide -Terminated Polymers. "Clicking" Polyelectrolyte Brushes on Planar Surfaces and Nanochannels. *Polym. Chem.* **2010**, *1* (2), 183−192.

DOI: 10.1021/acs.biomac.8b01346
Biomacromolecules 2019, 20, 769−777

(26) Griffo, A.; Hähl, H.; Grandthyll, S.; Müller, F.; Paananen, A.; Ilmén, M.; Szilvay, G. R.; Landowski, C. P.; Penttilä, M.; Jacobs, K.; Laaksonen, P. Single-Molecule Force Spectroscopy Study on Modular Resilin Fusion Protein. *ACS Omega* **2017**, *2* (10), 6906−6915.
(27) Abitbol, T.; Kloser, E.; Gray, D. G. Estimation of the Surface Sulfur Content of Cellulose Nanocrystals Prepared by Sulfuric Acid Hydrolysis. *Cellulose* **2013**, *20* (2), 785−794.
(28) Hoeger, I.; Rojas, O. J.; Efimenko, K.; Velev, O. D.; Kelley, S. S. Ultrathin Film Coatings of Aligned Cellulose Nanocrystals from a Convective-Shear Assembly System and Their Surface Mechanical Properties. *Soft Matter* **2011**, *7* (5), 1957−1967.
(29) Ahola, S.; Salmi, J.; Johansson, L.-S.; Laine, J.; Österberg, M. Model Films from Native Cellulose Nanofibrils. Preparation, Swelling, and Surface Interactions. *Biomacromolecules* **2008**, *9* (4), 1273−1282.
(30) Kontturi, E.; Meriluoto, A.; Penttilä, P. A.; Baccile, N.; Malho, J.-M.; Potthast, A.; Rosenau, T.; Ruokolainen, J.; Serimaa, R.; Laine, J.; Sixta, H. Degradation and Crystallization of Cellulose in Hydrogen Chloride Vapor for High-Yield Isolation of Cellulose Nanocrystals. *Angew. Chem., Int. Ed.* **2016**, *55* (46), 14455−14458.
(31) Herrera, M. A.; Mathew, A. P.; Oksman, K. Gas Permeability and Selectivity of Cellulose Nanocrystals Films (Layers) Deposited by Spin Coating. *Carbohydr. Polym.* **2014**, *112*, 494−501.
(32) Marko, J. F.; Siggia, E. D. Stretching DNA. *Macromolecules* **1995**, *28* (26), 8759−8770.
(33) Ott, W.; Jobst, M. A.; Bauer, M. S.; Durner, E.; Milles, L. F.; Nash, M. A.; Gaub, H. E. Elastin-like Polypeptide Linkers for Single-Molecule Force Spectroscopy. *ACS Nano* **2017**, *11* (6), 6346−6354.
(34) Sahlin, K.; Forsgren, L.; Moberg, T.; Bernin, D.; Rigdahl, M.; Westman, G. Surface Treatment of Cellulose Nanocrystals (CNC): Effects on Dispersion Rheology. *Cellulose* **2018**, *25* (1), 331−345.
(35) Börjesson, M.; Sahlin, K.; Bernin, D.; Westman, G. Increased Thermal Stability of Nanocellulose Composites by Functionalization of the Sulfate Groups on Cellulose Nanocrystals with Azetidinium Ions. *J. Appl. Polym. Sci.* **2018**, *135* (10), 45963.
(36) Kontturi, E.; Thüne, P. C.; Niemantsverdriet, J. W. Cellulose Model SurfacesSimplified Preparation by Spin Coating and Characterization by X-Ray Photoelectron Spectroscopy, Infrared Spectroscopy, and Atomic Force Microscopy. *Langmuir* **2003**, *19* (14), 5735−5741.
(37) Oun, A. A.; Rhim, J.-W. Effect of Oxidized Chitin Nanocrystals Isolated by Ammonium Persulfate Method on the Properties of Carboxymethyl Cellulose-Based Films. *Carbohydr. Polym.* **2017**, *175*, 712−720.
(38) Nelson, M. L.; O'Connor, R. T. Relation of Certain Infrared Bands to Cellulose Crystallinity and Crystal Lattice Type. Part II. A New Infrared Ratio for Estimation of Crystallinity in Celluloses I and II. *J. Appl. Polym. Sci.* **1964**, *8* (3), 1325−1341.
(39) Sajadi, E.; Babaipour, V.; Deldar, A. A.; Yakhchali, B.; Fatemi, S. S.-A. Enhancement of Crystallinity of Cellulose Produced by Escherichia Coli through Heterologous Expression of BcsD Gene from Gluconacetobacter Xylinus. *Biotechnol. Lett.* **2017**, *39* (9), 1395−1401.
(40) Poletto, M.; Ornaghi, H. L.; Zattera, A. J. Native Cellulose: Structure, Characterization and Thermal Properties. *Materials* **2014**, *7* (9), 6105−6119.
(41) Kraulis, P. J.; Clore, G. M.; Nilges, M.; Jones, T. A.; Pettersson, G.; Knowles, J.; Gronenborn, A. M. Determination of the Three-Dimensional Solution Structure of the C-Terminal Domain of Cellobiohydrolase I from Trichoderma Reesei. A Study Using Nuclear Magnetic Resonance and Hybrid Distance Geometry-Dynamical Simulated Annealing. *Biochemistry* **1989**, *28* (18), 7241−7257.
(42) Lehtio, J.; Sugiyama, J.; Gustavsson, M.; Fransson, L.; Linder, M.; Teeri, T. T. The Binding Specificity and Affinity Determinants of Family 1 and Family 3 Cellulose Binding Modules. *Proc. Natl. Acad. Sci. U. S. A.* **2003**, *100* (2), 484−489.
(43) Tormo, J.; Lamed, R.; Chirino, A. J.; Morag, E.; Bayer, E. A.; Shoham, Y.; Steitz, T. A. Crystal Structure of a Bacterial Family-III Cellulose-Binding Domain: A General Mechanism for Attachment to Cellulose. *EMBO J.* **1996**, *15* (21), 5739−5751.
(44) Reinikainen, T.; Ruohonen, L.; Nevanen, T.; Laaksonen, L.; Kraulis, P.; Jones, T. A.; Knowles, J. K. C.; Teeri, T. T. Investigation of the Function of Mutated Cellulose-Binding Domains of Trichoderma Reesei Cellobiohydrolase I. *Proteins: Struct., Funct., Genet.* **1992**, *14* (4), 475−482.
(45) Mattinen, M.-L.; Linder, M.; Teleman, A.; Annila, A. Interaction between Cellohexaose and Cellulose Binding Domains from Trichoderma Reesei Cellulases. *FEBS Lett.* **1997**, *407* (3), 291−296.
(46) Mendes, B. B. Human-based fibrillar nanocomposite hydrogels as bioinstructive matrices to tune stem cell behavior. *Nanoscale* **2018**, *10* (36), 17388−17401.
(47) Lin, N.; Dufresne, A. Surface Chemistry, Morphological Analysis and Properties of Cellulose Nanocrystals with Gradiented Sulfation Degrees. *Nanoscale* **2014**, *6* (10), 5384−5393.
(48) *Intermolecular and Surface Forces*; Elsevier: 2011.
(49) Kontturi, E.; Suchy, M.; Penttilä, P.; Jean, B.; Pirkkalainen, K.; Torkkeli, M.; Serimaa, R. Amorphous Characteristics of an Ultrathin Cellulose Film. *Biomacromolecules* **2011**, *12* (3), 770−777.
(50) Kikkawa, Y.; Tokuhisa, H.; Shingai, H.; Hiraishi, T.; Houjou, H.; Kanesato, M.; Imanaka, T.; Tanaka, T. Interaction Force of Chitin-Binding Domains onto Chitin Surface. *Biomacromolecules* **2008**, *9* (8), 2126−2131.
(51) Malho, J.-M.; Arola, S.; Laaksonen, P.; Szilvay, G. R.; Ikkala, O.; Linder, M. B. Modular Architecture of Protein Binding Units for Designing Properties of Cellulose Nanomaterials. *Angew. Chem., Int. Ed.* **2015**, *54* (41), 12025−12028.
(52) Varjonen, S.; Laaksonen, P.; Paananen, A.; Valo, H.; Hähl, H.; Laaksonen, T.; Linder, M. B. Self-Assembly of Cellulose Nanofibrils by Genetically Engineered Fusion Proteins. *Soft Matter* **2011**, *7* (6), 2402−2411.
(53) Oesterhelt, F.; Rief, M.; Gaub, H. E. Single Molecule Force Spectroscopy by AFM Indicates Helical Structure of Poly(Ethylene-Glycol) in Water. *New J. Phys.* **1999**, *1* (1), 6.

DOI: 10.1021/acs.biomac.8b01346
Biomacromolecules 2019, 20, 769−777